Angular Distributions for the Cl + C_2H_6 → HCl + C_2H_5 Reaction Observed via Multiphoton Ionization of the C_2H_5 Radical

S. Alex Kandel, T. Peter Rakitzis, Topaz Lev-On, and Richard N. Zare*

Department of Chemistry, Stanford University, Stanford, California 94305

Received: November 12, 1997; In Final Form: January 20, 1998

The title reaction has been studied by observing the ethyl radical product by means of resonance-enhanced multiphoton ionization (REMPI) that proceeds at 242 nm via highly dissociative Rydberg states. The method of core extraction was employed to measure the speed and spatial anisotropy distributions of the C_2H_5 product from which the differential cross section and the internal energy distribution of the products were deduced. The C_2H_5 product exhibits broad scattering that peaks sideways, and the internal modes of this product are not significantly excited. These results agree closely with those found from a previous study of the title reaction in which the HCl product was detected by REMPI under the same conditions. Additionally, we report REMPI detection of the propyl radical product in the analogous Cl + C_3H_8 reaction.

1. Introduction

In a previous publication,[1] we reported results detailing our investigation of the gas-phase reaction of atomic chlorine with ethane,

$$Cl(^2P_{3/2}) + C_2H_6 \rightarrow HCl(v, J) + C_2H_5$$

The reaction was studied using a photoinitated technique that employs energy- and momentum-conservation relations to extract state-specific angular scattering distributions in a "bulb-like" reaction environment. Experimental realization of this method requires the detection of one of the reaction products in a manner that is sensitive to both its internal state and its velocity.[2−4] This task was accomplished in the previous study through HCl (2+1) resonance-enhanced multiphoton ionization (REMPI), followed by detection using a velocity-sensitive mass spectrometer.

We recently observed that the focused 240 nm light used for HCl REMPI also ionizes the ethyl radical. This multiphoton ionization (MPI) of the C_2H_5 reaction product is dissociative and produces the parent ion, $C_2H_5^+$, as well as varying amounts of fragmentation products, from C_2^+ to $C_2H_4^+$. Until recently, we attributed these ions to a background interference resulting from ionization and fragmentation of the C_2H_6 reagent. Such reagent background interferences indeed exist, but simple subtraction procedures allow detection of C_2H_5 product alone.

In this paper, we report angular scattering and average product internal energy distributions derived from velocity-resolved MPI of the C_2H_5 radical. We compare these results with similar distributions derived from HCl REMPI measurements. We show that the results obtained from these two different detection methods are in excellent agreement, which provides a verification of the accuracy of our experimental technique. Additionally, we report our observation of C_3H_7 MPI and discuss the feasibility of using hydrocarbon radical MPI as a probe of chemical dynamics for a wide range of reactions.

2. Experimental Section

Techniques and Apparatus. We present here an overview of our experimental apparatus, as more detailed descriptions were provided in previous publications.[1,5] Ethane (99.99%), molecular chlorine (99.999%), and helium (99.995%) were premixed and expanded through a pulsed nozzle (General Valve 9-Series, 0.6 mm orifice, 0.5 atm backing pressure). The chemical reaction was initiated in the Cl_2/C_2H_6 expansion by the production of atomic chlorine via photolysis of the Cl_2 precursor at 355 nm (Nd^{3+}:YAG third harmonic), which produces >98% ground-state chlorine ($^2P_{3/2}$).[6] Products were allowed to build for 10−70 ns. C_2H_5 radicals were then detected using 0.2−1 mJ of 242.3 nm light from a frequency-doubled Nd^{3+}:YAG-pumped dye laser (LD 489 laser dye), at the focal point of a 1.1 m lens. The resulting ions were separated according to mass in a linear time-of-flight (TOF) mass spectrometer and detected on dual microchannel plates (MCPs).

To obtain product scattering information, we measured C_2H_5 product velocities through use of the core-extraction technique, which exploits the innate sensitivity of the TOF mass spectrometer to the initial velocity of the detected ions.[5] The distribution of C_2H_5 speeds, which remains essentially unchanged in the ionization process, results in a spreading of the ions as they travel through the mass spectrometer toward the detector. The resulting ion-arrival profile is similar to a Doppler-broadened line shape and can be analyzed to yield the ethyl speed distribution. This speed distribution of reaction products can be converted directly to the center-of-mass differential cross section, provided the relative velocity between reagents is specified and the state-to-state energetics of the system are known.

Ionization of C_2H_5 seems insensitive to internal state, as will be discussed presently. Therefore, the state-to-state energetics of the reaction cannot be determined exactly. This lack of information introduces ambiguity into the transformation from the measured speed distribution to the differential cross section. We can resolve much of this ambiguity with a coincident determination of the product translational energy release, which is afforded by the measurement of the C_2H_5 spatial distribution. Chlorine atom reagents produced by Cl_2 photolysis are formed in a $\sin^2\theta$ distribution about the direction of the photolysis polarization vector. The deviation from this behavior in the C_2H_5 spatial distribution is directly related to the laboratory-frame angle between the velocities of the incident chlorine atoms and the ethyl radicals, and this angle can be inverted to yield

S1089-5639(98)00182-0 CCC: $15.00
Published on Web 03/06/1998

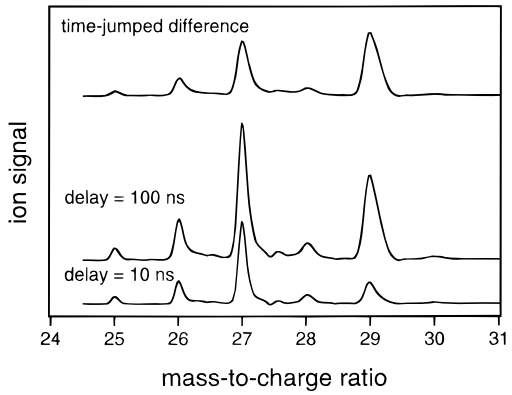

Figure 1. Mass spectrum of hydrocarbon fragment ions produced by the 242 nm probe laser from nonresonant ionization of the C_2H_6 reagent and from ionization and dissociative ionization of the C_2H_5 radical reaction product from $Cl + C_2H_6$. Mass spectra were acquired for short (10 ns) and long (100 ns) delays between the photolysis and probe lasers. At the short delay, the majority of ions produced are background signals from ethane ionization. At the long delay, there is significant contribution from MPI of the C_2H_5 product. The subtracted difference trace measures the ethyl radical reaction product alone. Traces are offset vertically for clarity of presentation.

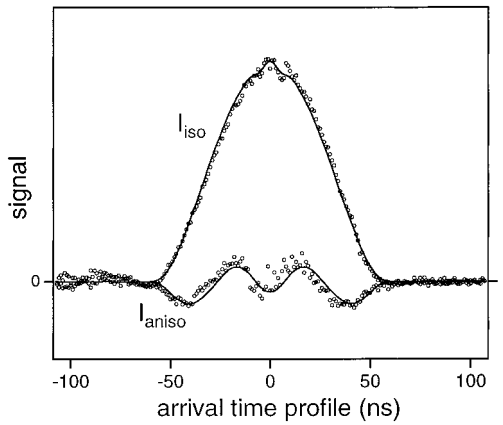

Figure 2. Composite ion-arrival profiles of the C_2H_5 radical product from the $Cl + C_2H_6$ reaction. These composite profiles are composed of experimental signals recorded with the photolysis laser polarization vector parallel and perpendicular to the detection axis. An isotropic sum, $I_{iso} = I_{||} + 2I_{\perp}$, removes spatial anisotropy resulting from the Cl_2 photodissociation. The anisotropic difference, $I_{aniso} = 2(I_{||} - I_{\perp})$, is linearly dependent on the product spatial anisotropy.

the translational energy of the reaction products. Details of this transformation are presented in section 3. We measured the ethyl radical spatial distribution by acquiring ion arrival profiles with the photolysis polarization vector parallel and perpendicular to the TOF axis. This polarization change was effected on a shot-to-shot basis through the use of a photoelastic modulator (Hinds International PEM-80) in the photolysis laser beam path.

All measurements presented here required a background correction to remove interferences originating from C_2H_6 dissociative ionization by the focused 242 nm probe light. To ensure that only reactive products were measured, we used a time-jump subtraction method. In this subtraction procedure, ion signals are measured while the delay between the photolysis and probe lasers is altered from 10 to 70 ns. Subtraction of these signals removes all backgrounds that do not increase with the photolysis-probe delay, and we detect only products that result from reaction in the 60 ns differenced time interval. This time difference was switched every other laser shot by directing the photolysis Q-switch signal alternately through a varying cable delay.

Characterization of C_2H_5 MPI. Figure 1 presents TOF mass spectra of the ions produced using focused 242 nm light to probe the C_2H_5 radical. These TOF mass spectra illustrate the use of the time-jump subtraction to eliminate nonreactive backgrounds. The spectra were recorded for short (10 ns) and long (100 ns) delays between the photolysis and probe lasers and are shown along with a subtracted TOF trace, which discriminates only ions resulting from MPI of C_2H_5 reaction products. These spectra were recorded using a large extraction field to collect all ions produced, irrespective of their initial velocities. We see that MPI of C_2H_5 results in an assortment of charged species, which includes the parent $C_2H_5^+$ ion as well as $C_2H_x^+$ ionic fragments: $C_2H_5^+$ and $C_2H_3^+$ signals dominate the spectrum. As probe laser power increases, all fragment ion signals increase in intensity relative to the $C_2H_5^+$ peak, though the branching into different fragment channels seems largely power independent. Neither this fragmentation pattern nor the total ionization efficiency appeared to change as a function of probe wavelength, which was sampled at several points between 240 and 250 nm. More importantly, we observed that the C_2H_5 ion-arrival profile, from which the product speed distribution and scattering are deduced, is identical over a range of probe powers and excitation wavelengths.

The C_2H_5 radical exhibits a broad absorption spectrum at wavelengths shorter than 260 nm, which is associated with a Rydberg progression of states, in which little or no rotational or vibrational structure is apparent.[7] Additionally, C_2H_5 dissociation has been observed experimentally through the 3s state at 248 nm.[8] We propose that our observed ionization of the ethyl radical at 242 nm proceeds via a 1 + 1 REMPI process mediated by the 3s Rydberg state. A similar ionization process has been reported for 1 + 1 REMPI via the 3s state of the methyl radical at 216 nm.[9] The dissociative nature of the C_2H_5 excited electronic state is in accordance with the lack of structure observed in the MPI process, the fragmentation that accompanies ionization, and the relatively small amounts of $C_2H_5^+$ ion signal. These factors lead us to assume also that the MPI process is insensitive to the internal state of the C_2H_5 radical.

It is important to note that we expect the ethyl radical reaction products to have small amounts of internal energy, as the $Cl + C_2H_6$ reaction is only slightly exothermic and is studied here at low collision energies. The MPI process could proceed differently for ethyl radicals with significant internal excitation, as these radicals might be expected to fragment more readily during ionization. Thus, we will not extend the assumption of internal-state insensitivity to highly excited C_2H_5.

3. Results

Core-extracted ion arrival profiles were recorded with the photolysis laser polarization vector pointing parallel and perpendicular to the TOF axis. We refer to these two profiles as $I_{||}$ and $I_{\perp}$. Spatial anisotropy in the experiment originates solely from the Cl_2 photodissociation, which has a $\sin^2\theta$ distribution ($\beta = -1$) for production of $Cl(^2P_{3/2})$. Consequently, measurements using these two polarization geometries are sufficient to determine the three-dimensional velocity distribution of the C_2H_5 products. Analysis of the raw data proceeds through the formation of composite profiles, $I_{iso} = I_{||} + 2I_{\perp}$ and $I_{aniso} = 2(I_{||} - I_{\perp})$, which are shown in Figure 2. These profiles are fit by summations of basis functions, in which each basis function simulates the instrumental response to products moving at a single speed with a maximal spatial anisotropy. Fitting of the data is accomplished through the use of a maximum-entropy

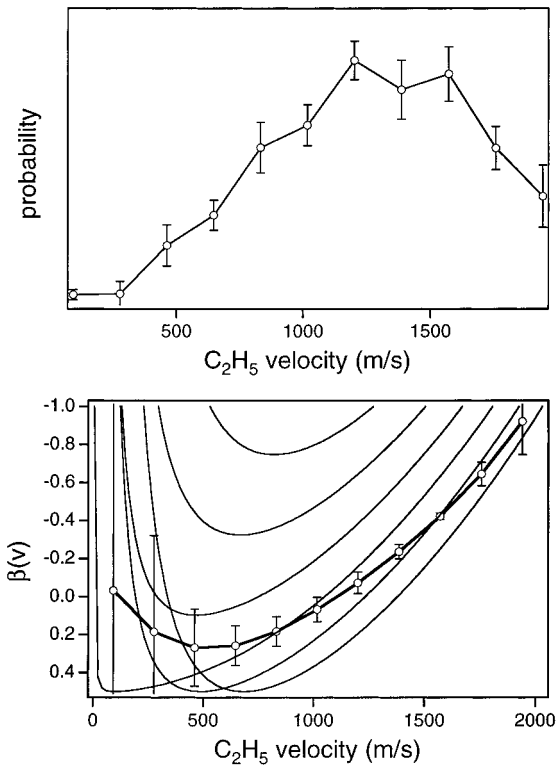

Figure 3. Speed distribution and speed-dependent spatial anisotropy for the C_2H_5 reaction product. Error bars are 1σ and are determined via statistical analysis of replicate measurements. The spatial anisotropy is plotted along with calculated curves that depict how spatial anisotropy varies with speed for differing amounts of internal energy in the reaction products. Contours are drawn for every 500 cm^{-1} of internal excitation.

analysis of the I_{iso} profile, which yields the product speed distribution, followed by a least-squares procedure for the I_{aniso} profile, from which the speed-dependent spatial anisotropy is obtained.[1,5,10] Speed and spatial anisotropy distributions for the ethyl radical product are shown in Figure 3. The speed distribution and speed-dependent spatial anisotropy are presented with 1σ error bars derived from statistical analysis of replicate measurements.

Previous publications have detailed the relationship between product spatial anisotropy and internal energy.[1,2,5,10] Briefly, the spatial anisotropy of the product is derived from the chlorine atom spatial anisotropy but is rotated and averaged according to the extent by which reagent and product laboratory-frame velocities, v_{Cl} and v_{prod}, deviate. We define α as the angle between these velocities, and we present the following expression:

$$\beta_{prod}(v_{prod}) = \beta_{Cl} P_2(\cos \alpha) \quad (1)$$

where

$$P_2(\cos \alpha) = \frac{1}{2}(3 \cos^2 \alpha - 1) \quad (2)$$

The angle α can be related directly to the product speed measured in the laboratory, v_{prod}, the center-of-mass speed, v_{com}, and the product speed in the center-of-mass frame, u_{prod}:

$$\cos \alpha = \frac{v_{prod}^2 + v_{com}^2 - u_{prod}^2}{2 v_{prod} v_{com}} \quad (3)$$

When the internal energy of both reaction products is known, conservation of energy determines u_{prod}. In the current experiment, C_2H_5 detection is state-insensitive; furthermore, the HCl product is formed with a range of internal energies. Therefore, it is possible for observed C_2H_5 products moving at a single laboratory-frame velocity to have a distribution of product center-of-mass speeds. Equation 1 is thus necessarily reexpressed as a weighted integral:

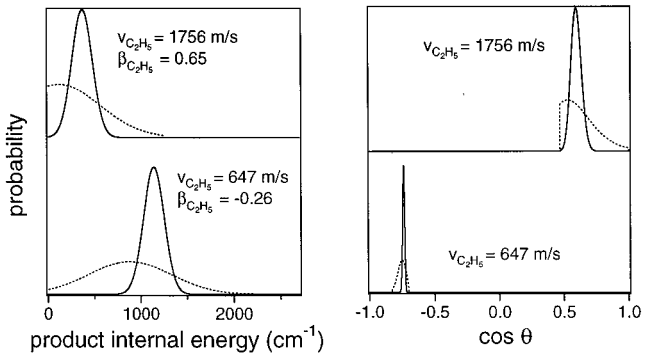

Figure 4. Simulation of the effect of the product internal energy distribution on our analysis. The left panel shows narrow and broad energy distributions simulated for fast (1756 m/s) and slow (647 m/s) speeds. Both distributions for the fast products yield an average spatial anisotropy, $\beta = 0.65$, and both distributions for slow products yield $\beta = -0.26$. These distributions would therefore not be experimentally distinguishable. By observing the differences in resulting scattering, shown in the right panel, we can approximate the dependence of our analysis on the functional form of the product internal energy distribution.

$$\beta_{prod}(v_{prod}) = \beta_{Cl} \int P_2\left(\frac{v_{prod}^2 + v_{com}^2 - u_{prod}^2}{2 v_{prod} v_{com}}\right) N(u_{prod}, v_{prod})\, du_{prod} \quad (4)$$

where the proportion of products with laboratory speed v_{prod} that result from product center-of-mass velocity u_{prod} is given by $N(u_{prod}, v_{prod})$. For cases in which the distribution of product center-of-mass speeds is tightly peaked about a single value (resulting from a tightly peaked distribution of product internal states), a measurement of β_{prod} yields a good approximation of u_{prod} using eq 1. It is then straightforward to calculate the product internal energy and to invert v_{prod} to the center-of-mass scattering angle, θ. Often, however, the distribution of product internal states is not known and may not be sharply peaked.

Figure 4 shows a simulation that demonstrates the effect of the product internal energy distribution on our analysis for fast (1756 m/s) and slow (647 m/s) product speeds. We simulate narrow and broad energy distributions for each speed, and we select these distributions so that the average spatial anisotropy is identical. Thus, for a given speed, products scattering with either of these energy distributions are experimentally indistinguishable. When we examine the scattering resulting from narrow and broad energy distributions, we find that our lack of knowledge of the product internal energy does not severely affect our results. For fast products, a broad internal energy distribution results in a spread of scattering angles, indicating that our inversion of product speed to scattering may slightly overestimate our experimental resolution in the forward-scattered region. For the slower products shown, scattering is far less dependent on product internal energy; however, the inversion of $\beta(v)$ to obtain the average product energy may suffer in this region. In general, a combined analysis utilizing both speed and spatial anisotropy measurements is likely to produce the correct differential cross section and to provide an approximation of the product internal energy.

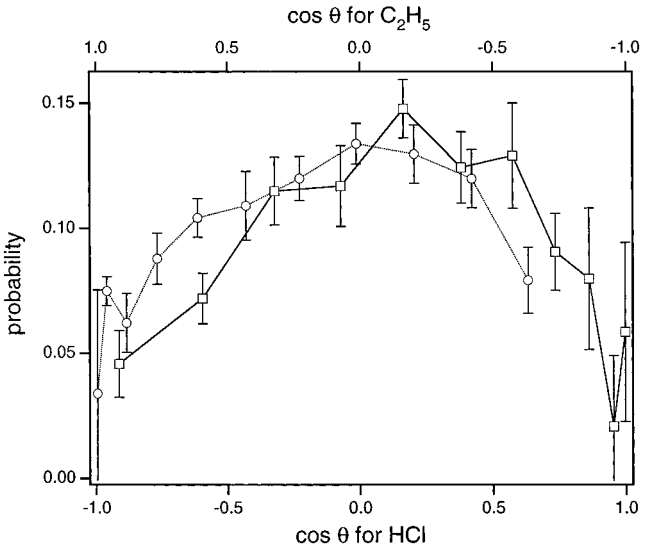

Figure 5. Center-of-mass differential cross sections for the $Cl + C_2H_6$ reaction. These cross sections are inverted from speed and spatial anisotropy distributions of the HCl product (taken from ref 1, circles and dotted lines, bottom axis) and the C_2H_5 product (from this work, squares and solid lines, top axis). The figure is constructed so that products resulting from similar collisions are superimposed. We define the center-of-mass scattering angle θ to be relative to the chlorine atom reagent velocity vector; thus, cos θ takes opposite signs for HCl and C_2H_5 products.

We use the measured C_2H_5 spatial anisotropy to approximate the product center-of-mass velocity and thus transform the speed distribution to the differential cross section. We perform a similar analysis on previously published[1] speed and anisotropy distributions for the HCl products of this reaction. Although we observe changes in HCl scattering for high rotational states of HCl, the vast majority of collisions produce rotationally cold HCl(v=0). We estimate that approximately 0.3% of the HCl product is vibrationally excited. Thus, the overall scattering for the reaction is well described by the scattering of HCl-(v=0,J=1). We compare the differential cross section for HCl-(v=0,J=1) with the C_2H_5 differential cross section in Figure 5. Scattering for both products is described relative to the Cl reagent velocity. The horizontal scales for the two products are reversed relative to one another, so that products arising from similar reactive collisions are shown superimposed on the graph. Error bars on both cross sections are 1σ statistical deviations. The degree of correspondence between the two cross sections is excellent. A reactive collision that produces forward-scattered HCl necessarily produces backward-scattered ethyl radical, and thus the HCl products with the largest laboratory-frame velocity are formed in the same collisions as the ethyl radical products with the smallest laboratory-frame velocity, and vice versa. Hence, agreement between the two cross sections indicates that no velocity-dependent experimental bias exists in our apparatus. Furthermore, the similarity of these data rules out bias resulting from the detection technique. The agreement between the HCl and C_2H_5 differential cross sections provides the strongest justification for our experimental and analysis procedures that we have yet reported.

We have also observed C_3H_7 product from the $Cl + C_3H_8$ reaction. We propose that propyl radical MPI occurs through a similar REMPI mechanism mediated by the 3p Rydberg state. Interpretation of the C_3H_7 data is complicated by the presence of both primary and secondary hydrogens in the propane reagent. A qualitative analysis, however, yields broad scattering that slightly favors backscattered and side-scattered trajectories. This result is in rough agreement with that reported by Varley and Dagdigian for HCl and DCl products from $Cl + CD_3CH_2CD_3$.[11]

4. Discussion

We have observed MPI of C_2H_5 reaction products from the $Cl + C_2H_6$ reaction at a collision energy of 0.24 eV. We believe that this observed ionization is caused by a highly dissociative 1 + 1 REMPI process mediated by the 3s Rydberg state of the ethyl radical. We have used the method of core extraction to measure speed and spatial anisotropy distributions for the radical products of this reaction, and we have detailed the means by which these data can be used in concert to arrive at the internal energy of the products as well as the center-of-mass differential cross section. We have compared the resulting differential cross section for $Cl + C_2H_6$ to that obtained via earlier measurements of the HCl product. We find excellent agreement.

Our previous interpretation of the $Cl + C_2H_6$ reaction used the line-of-centers model to describe the opacity function for the reaction; a hard-sphere scattering model was then employed to predict differential cross sections.[1] These models predict a flat differential cross section that falls off sharply at cos θ = 0.9. The broad scattering we observed is in qualitative agreement with this prediction. The measured scattering, however, shows a wide but distinct peak for side-scattered products, falling off in the forward and backward regions. Because we have now observed identical behavior in the C_2H_5 differential cross section in this study, we are fully confident that this scattering is indeed a dynamical effect in this reaction. Departure from the very simple models used is hardly surprising. We find it likely that effects such as nonspecular scattering and impact-dependent angular acceptance could produce such behavior.

Hydrocarbon radical MPI might be a means of probing a variety of other reactive processes. The large amount of dissociation accompanying ionization certainly limits the sensitivity of the technique. Signal levels were more than adequate for the current study; however, reactions of chlorine atoms with hydrocarbons generally proceed with large cross sections. Significant gains in sensitivity would be expected from the use of higher probe powers along with gentler focusing of the light. Detection of hydrocarbon radicals might be further facilitated through the use of bright light sources at 212 or 248 nm.

Acknowledgment. S.A.K. thanks the National Science Foundation for a predoctoral fellowship. S.A.K. also gratefully acknowledges receipt of a Dr. Franklin Veatch Memorial fellowship. This work has been supported by the National Science Foundation under Grant CHE-93-22690.

References and Notes

(1) Kandel, S. A.; Rakitzis, T. P.; Lev-On, T.; Zare, R. N. *J. Chem. Phys.* **1996**, *105*, 7550.

(2) Shafer, N. E.; Orr-Ewing, A. J.; Simpson, W. R.; Xu, H.; Zare, R. N. *Chem. Phys. Lett.* **1993**, *212*, 155.

(3) Aoiz, F. J.; Brouard, M.; Enriquez, P. A.; Sayos, R. J. *J. Chem. Soc., Faraday Trans.* **1993**, *89*, 1427.

(4) Kim, H. L.; Wickramaaratchi, M. A.; Zheng, X.; Hall, G. E. *J. Chem. Phys.* **1994**, *101*, 2033.

(5) Simpson, W. R.; Orr-Ewing, A. J.; Kandel, S. A.; Rakitzis, T. P.; Zare, R. N. *J. Chem. Phys.* **1995**, *103*, 7299.

(6) Matsumi, Y.; Tonokura, K.; Kawasaki, M. *J. Chem. Phys.* **1992**, *97*, 1065.

(7) Wendt, H. R.; Hunziker, H. E. *J. Chem. Phys.* **1984**, *81*, 717.

(8) Brum, J. L.; Deshmukh, S.; Koplitz, B. *J. Chem. Phys.* **1991**, *95*, 2200.

(9) Danon, J.; Zacharias, H.; Rottke, H.; Welge, K. H. *J. Chem. Phys.* **1982**, *76*, 2399.

(10) Simpson, W. R.; Rakitzis, T. P.; Kandel, S. A.; Orr-Ewing, A. J.; Zare, R. N. *J. Chem. Phys.* **1995**, *103*, 7313.

(11) Varley, D. F.; Dagdigian, P. J. *Chem. Phys. Lett.* **1996**, *255*, 393.